# MECHANISMS OF OIL RECOVERY BY CARBONATED WATER INJECTION

Mehran Sohrabi, Masoud Riazi, Mahmoud Jamiolahmady,
Shaun Ireland and Chris Brown
Institute of Petroleum Engineering, Heriot-Watt University, Edinburgh, UK

*This paper was prepared for presentation at the International Symposium of the Society of Core Analysts held in Noordwijk, The Netherlands 27-30 September, 2009*

## ABSTRACT

CO2 injection is a proven technology for enhanced oil recovery (EOR). It is well known that the low viscosity of CO2 and hence its high mobility in oil reservoirs adversely affects the sweep efficiency during CO2 injection. To alleviate this problem, various injection strategies e.g. gravity stable, alternating and simultaneous injection of water and CO2 have been suggested and studied. An alternative injection strategy that can eliminate many of the shortcomings of direct CO2 injection is carbonated water injection (CWI). CWI also provides a very safe method for storing large quantities of CO2 as a dissolved phase in oil reservoirs.

This paper presents part of the results of an ongoing joint industry research to investigate the performance of CWI as an enhanced oil recovery method. Using the results of high-pressure direct flow visualisation (micromodel) experiments, we reveal the pore-scale mechanisms of oil recovery by CWI. CWI improved the recovery of both light and heavy oil albeit through different mechanisms. The additional oil recovery in light oil was mainly due to high dissolution of CO2 in the oil and high oil swelling factor. The viscous oil exhibited a lower swelling factor but a higher viscosity reduction. In both light and viscous oil, CWI recovered more oil compared to unadulterated water flooding.

## INTRODUCTION

CO2 injection for EOR is a well-established technology which has been extensively applied to onshore conventional (light) oil reservoirs. The application of CO2 for EOR has so far been limited to a few countries mainly the USA and Canada where natural resources of CO2 have been available. Recently there has been a renewed interest globally in CO2 injection in oil reservoirs for both EOR and CO2 storage purposes.

The main advantage of CO2 is that at most conventional oil reservoirs conditions it is a supercritical fluid and is very likely to develop miscibility with the oil. Immiscible CO2 injection has also been shown to increase oil recovery by primarily altering the physical properties of the oil as a result of mixing with CO2. At conditions of typical oil reservoirs, significant quantities of CO2 can dissolve in oil leading to oil swelling and

subsequently reduction in the oil viscosity. Extraction of crude oil components can also take place resulting in evaporation of the light and intermediate components of crude oil. This extraction mechanism increases the production of lighter and intermediate components of the oil but the remaining oil will become increasingly more viscous and hence more difficult to produce. The remaining heavier components of the oil such as waxes and asphalts can also cause pore blockage and permeability reduction making the flow and production of the remaining oil increasingly difficult. It has also been reported that poor sweep efficiency has been a problem in CO2 floods of many oil reservoirs (Patel et al., 1987). Poor sweep efficiency significantly limits the contact between the resident oil and the injected CO2 hence reducing CO2 flood performance. It also has a significant adverse effect on the economy of CO2 flood projects as it leads to low oil recovery and premature CO2 breakthrough requiring significant CO2 separation and re-injection. The presence of water layers between isolated oil ganglia in tertiary (post waterflood) CO2 injection is also believed to negatively impact CO2 performance. This so-called water shielding or water blocking effect can prevent direct contact between the oil and CO2 and hence reducing the rate of CO2 dissolution in the oil. The effect has been studied experimentally (Philip and Kishore, 1997), visually (Campbell, et al., 1985) and theoretically (Grogan, et al., 1987, 1988, Do and Pinczewski, 1993 and Bijeljic, et al., 2002).

Therefore, direct injection of CO2 might not result in economically significant amount of additional oil recovery. From CO2 storage perspective, storing CO2 as a free phase in a reservoir can pose significant leakage risk. An alternative CO2 injection strategy that can eliminate many of the shortcomings of direct CO2 injection is carbonated (CO2-enriched) water injection (CWI). Compared to CO2 injection, carbonated water has a much better sweep efficiency and a much slower CO2 breakthrough because its mobility is essentially that of water. CWI also alleviates the adverse effect of high water saturation and the water shielding effects as a result of mixing with the resident water which facilitates CO2 dissolution and the subsequent oil swelling. In direct CO2 injection, it has been shown that, due to low sweep efficiency and gravity segregation, the time scale for CO2 diffusion in oil can be several years (Solomon, 2007).

The objective of the ongoing Carbonated Water Injection JIP (joint industry project) at Heriot-Watt University is to investigate the application of CO2-enriched water injection as an injection strategy for enhanced oil recovery and CO2 storage using an integrated experimental and theoretical approach. In this paper we present some of the results of our direct flow visualisation experiments which were carried out as part of a comprehensive series of experiment that are being performed in this project.

## EXPERIMENTAL FACILITIES

***High-pressure Micromodel Rig.*** A high-pressure micromodel rig has been used for performing carbonated water injection tests reported in this paper. The rig was capable of operating at pressures as high as 6000 psia (41.37 MPa), however, the experiments

reported here were conducted at 2000 psia (13.8 MPa) and 38 °C (100.4 °F). The rig is equipped with an optical system which allows a camera and its lens to be positioned at any part of the micromodel. While running a test, the optical system is used for scanning the micromodel for obtaining high-quality still images as well as recording videos of fluid flow and displacement events. These images and videos are then used for the purpose of analysing the fluid flow mechanisms and also for quantifying the fluid saturation at various stages of experiments. The details of micromodel, high pressure rigs and optical system have been reported elsewhere in our previous publications (Sohrabi *et al.*, 2000, 2004, 2007, 2008a, 2008b).

**Fluids**

The fluid system used in the experiments consisted of two different types of oil (*n*-Decane and a viscous mineral oil), distilled water and carbon dioxide. The viscosity of the mineral oil at atmospheric pressure and the temperature of the experiments (38 ºC) was 16.5 mPa.s (cP) whereas the viscosity of *n*-Decane, which was used as a lighter oil compared to the mineral oil, was 0.83 mPa.s (cP) at 2000 psia and 38°C (National Institute of Standard and Technology). Carbonated water was prepared by mixing degassed water with pure CO2 in a rocking cell at 38 °C and 2000 psia. To distinguish between the oil and the aqueous phase, the colour of the water was changed to blue by adding a water-soluble (0.6% wt/wt) blue dye.

## RESULTS AND DISCUSSION

In the tests reported here, to minimise the gravity effect, the micromodel was mounted horizontally. Figure 1 shows the micromodel at the beginning of a typical test when fully saturated with blue water. The Figure shows the pore pattern as well as the triangles at either end of the porous section, which have been designed to evenly distribute the fluids in the porous medium. Figure 2 shows a section of the micromodel at higher magnification to show in more details the pore pattern of the micromodel used in this study. In both of these Figures, the blue areas represent the pores and the white areas are unetched glass representing rock grains. The dimensions of the porous section as well as the size of the pores are given in Table 1. All fluid displacements stages of the tests were carried out at the same slow rate of 0.1 $cm^3$ $h^{-1}$ corresponding to a low capillary number of 5E-7. The experiments commenced by saturating and pressurising the micromodel with water. Then, to simulate the primary drainage of water and the initial migration of oil in a reservoir, the oil phase was injected at a very slow rate of 0.1 $cm^3$ $h^{-1}$ from one end of the horizontal micromodel. The injection of oil stopped when the oil front reached the other end of the micromodel.

Two experiments are reported here. One with *n*-decane representing a light oil and the other one with a viscous oil with the aim of investigating oil recovery mechanisms during CWI for different oil types.

**Light Oil Recovery by CWI**

Figure 3, shows fluid distribution in a section of the micromodel at the end of the oil (*n*-decane) injection period at the beginning of the test. To better differentiate between the unetched glass and the oil, in this image and the following ones, the unetched glass has been shown as hatched areas. Figure 3 shows the relative position of the wetting phase (blue water) and non-wetting phase (*n*-decane) in the porous medium. Glass is water-wet and as a result, the water in the micromodel occupies the smaller and dead-end pores and also as layers on the walls of the oil-occupied pores. The shape and the direction of the water-oil interfaces are also good indications of water-wet conditions of the micromodel.

After establishing the initial oil and water saturations, water was injected into the micromodel at a low rate of 0.01 $cm^3$ $h^{-1}$ corresponding to a superficial velocity of 0.7 $md^{-1}$ and an actual (pore) velocity of around 3 $md^{-1}$. The actual velocity was estimated from the time it took for the water front to travel the length of the micromodel during water injection. Figure 4 illustrates the distribution of oil and water after water flooding. As can be seen, water has displaced part of the oil and has left behind some oil in the form of isolated oil ganglia. The oil production during water flooding took place mainly before the water breakthrough (BT). After BT, the flood water passed through the porous medium via the water films that already had been formed and left the model without any further oil recovery or fluid distribution. The displacement of oil by water during water flooding happened by film flow as well as piston type displacement. The water films surrounding the oil were observed to become progressively thicker as the water injection progressed and eventually caused disconnection of the oil by snap-off mechanism. The arrow in Figure 4 shows an isolated oil ganglion and the narrowing of oil, which caused by film flow displacement mechanism.

The saturation of the oil in the whole of the micromodel at various stages of the tests was estimated by measuring the number of pixels making the area of the oil divided by the total pore area of the micromodel. Since the depth of all pores in are the same, area ratio is equal to volume ratio. The error in the reported values of saturation is estimated to be +/-10%. The estimated data show that as a result of the first water injection period, the initial oil saturation reduced from 67% to 49%, which showed 18% oil production corresponding to a 26.9% oil recovery factor.

After establishing residual oil saturation by water flooding, CW (carbonated water) injection began with the direction of flow being the same as the preceding water flood and with the same rate of injection (0.01 $cm^3 h^{-1}$). When CW came in contact with oil and water in the micromodel, partitioning of CO2 from CW and its diffusion and dissolution into the oil phase took place. As a result, the isolated oil ganglia (Figure 4) swelled and consequently displaced some of the aqueous phase from the pores which led to reconnection of some of the isolated oil ganglia which were formed in the previous water flooding. The amount of oil swelling, which is a function of the oil type

and CO2 concentration in the CW, controls the coalescence mechanism of the disconnected oil ganglia. During the CWI (carbonated water injection) in this test significant swelling and coalescence of the trapped oil (n-decane) and its subsequent mobilisation and recovery was observed. The additional oil recovery took place gradually during the course of CWI. Figure 5 shows a snapshot of a section of the micromodel at the end of CWI, after about 144 hrs.

Comparison of Figure 5 with Figure 4 shows significant changes in fluid distribution within the micromodel caused by carbonated water injection including oil swelling and coalescence and displacement of the oil and water in the dead end pores. In this Figure, the red arrow points at an example of swelling of an oil ganglion and the green arrow (on the left hand side of the picture) shows the displacement of water from some dead-end pores as a result of the oil swelling. The displacement of water from the dead-end pores could only happen by counter current flow of oil and water which indicates that the swelling of the oil provided enough energy to overcome capillary forces in these pores. Favourable changes in interfacial tension (Daoyong Y. et al., 2005) and/or wettability (Chiquet, P. et al., 2005) during dissolution of CO2 can facilitate these displacements. The oval shape in Figure 5 shows an example of coalescence of the disconnected oil ganglia as a result of the oil swelling and water displacement. The rectangular shape shows the disconnection of an oil ganglion due to the oil displacement and its recovery. The saturation of the oil (mixture of oil and CO2) in the micromodel at the end of CWI period was estimated at 64%, which was very close to the initial (before water flood) oil saturation of 67%.

After the CWI period, since the remaining oil was a mixture of the oil and CO2, (plain) water was injected in the micromodel to strip CO2 from oil. This second water injection (WI) period was carried out to obtain the equivalent dead-oil volume of the oil remaining in porous medium after CWI in order to obtain the actual oil recovery due to CWI. The dead-oil saturation and distribution at the end of the second WI period is shown in Figure 6. Comparison of Figure 6 with Figure 5 clearly shows significant reduction in the oil volume and fragmentation due to shrinkage caused by stripping the dissolved CO2. Comparison of fluid saturation after the first WI (Figure 4) and the second WI (Figure 6) reveals that significant additional oil recovery took place during CWI which had been carried out after the first WI. The oil saturation at this point was estimated at 33%, which indicates 16% additional oil production. In other words, 32.7% of the oil which had been left behind after the initial water flooding had been recovered during the CWI period.

**Viscous Oil Recovery by CWI**

This experiment was carried out to investigate the performance of CWI in viscous oil and to compare the results with the observations made in the light oil (*n*-decane) experiment. The viscous oil used in the experiment was a hydrocarbon based refined oil with an initial viscosity of 16.5 cP at the conditions of the experiment. For consistency,

the same micromodel and aqueous phase was used and the experiment was carried out under the same conditions of pressure and temperature as the previous light oil experiment.

The test started with an oil injection period in the water-saturated micromodel to establish the initial oil and water saturations. Figure 7 shows fluid distribution after the oil injection stage. Comparison of the initial oil saturation and distribution of viscous oil in this test (Figure 7) with its corresponding stage in light oil (Figure 3), shows a very similar fluid distribution and saturation within the micromodel. Nevertheless, a higher initial oil saturation value was achieved in this test (76.4 %) compared to the light oil test (67 %) mainly due to a 20 times increased in the oil viscosity. After establishing the initial oil and water saturations, an initial water injection was carried out with the same injection rate as the previous test, 0.01 $cm^3$ $h^{-1}$. Figure 8 shows the distribution of viscous oil and water after this initial water injection. Comparison of fluid distribution in Figures 7 and 8 shows some viscous oil displacement and recovery due to waterflooding. Water injection resulted in larger trapped oil ganglia after WI in the viscous oil (Figure 8) compared to light oil (Figure 4). Around 19.7% of the oil was recovered during this stage leaving behind 56.7% trapped in the porous medium, compared to 49% water flood residual oil saturation in the light oil experiment. After this initial WI (water injection), CW was injected through the micromodel at a rate of 0.01 $cm^3$ $h^{-1}$. Figure 9 shows the fluid distribution in a section of the micromodel at the end of CWI.

During CWI, the viscous oil was observed to swell as CO2 departed from the flowing CW and dissolved in the oil. Comparison of fluid distribution, the sizes and the shapes of the oil ganglia in Figure 9 with Figure 8 clearly shows swelling of the viscous oil during CWI. The arrow in Figure 9 shows an example of an isolated oil ganglion, which has swollen compared to its size in Figure 8. This swelling caused oil reconnection followed by remobilisation and recovery of some of the trapped oil. The red rectangle in Figure 9 illustrates an obvious oil displacement when compared with the same spot in the micromodel after WI period (Figure 8). The amount of the oil swelling observed in the viscous oil case was less than the light oil and hence less oil reconnection and remobilisation took place during viscous oil test. This was mainly due to the fact that CO2 solubility in oil reduces as the oil viscosity increases.
At the end of CWI, the saturation of the remaining oil (mixture of viscous oil and dissolved CO2) was estimated to be 61.4%. Similarly to the light oil experiment, in this experiment again a second water injection period was carried out after CWI in order to slowly strip the dissolved CO2 from the oil and obtain the dead-oil saturation.

Figure 10 shows the dead oil at the end of the second water injection period. Comparison of Figure 10 ($2^{nd}$ WI) with Figure 8 ($1^{st}$ WI) shows significant difference in fluid distribution and saturation as a result of the CWI period. The red rectangle in Figure 10 highlights that a previously large trapped oil ganglion remaining after the initial water injection period (shown by the arrow in Figure 8) has now have a smaller volume (oil

production) as well as being broken into several pieces. The residual oil saturation in this stage estimated to be 50%, which shows 6.7% PV additional oil production corresponding to 11.8% recovery from the waterflood residual oil.

Comparison of Figure 6 and Figure 5 with their corresponding stages in the viscous oil (Figure 9 and Figure 10) reveals much higher shrinkage of the oil after striping the dissolved CO2 in the case of light oil (*n*-decane) compared to what was observed for the viscous oil. The number of oil ganglia in the micromodel after the second WI in the light oil test (Figure 6) was about 50, however the corresponding number for the viscous oil test was just about 15. This difference confirms higher light oil shrinkage as a result of the stripping of the dissolved CO2 which, as expected, indicate higher CO2 solubility for the light oil.

### 3.3 Light Oil versus Viscous Oil

Two main mechanisms of oil recovery during carbonated water injection are; oil swelling and subsequent flow diversion and coalescence of the trapped oil ganglia, and the reduction in oil viscosity. The former is the dominant mechanism in light oil due to higher CO2 solubility and the latter is more relevant to viscous oil due to significant reduction in viscosity of these oils as a result of CO2 dissolution.

Figure 11 and Figure 12 show a summary of the oil saturation data estimated at the end of various stages of the experiments with the corresponding recovery factors. The data show that for both *n*-decane (light oil) and the viscous oil, the injection of carbonated water resulted in more oil recovery over and on top of what had already been recovered during water flooding. However, recovery factor for *n*-decane (32.7%) was much more than the viscous oil (11.8%). The higher oil recovery observed during the light oil CWI experiment is mainly attributed to the observed higher oil swelling and coalescence in this oil compared to the viscous oil. The Oil swelling factor can be calculated for the whole of micromodel using the oil saturation values at the end of the CW and the second WI periods. Based on the data plotted in Figures 11 and 12 the swelling factor of the light oil is about 94% and the corresponding value for the viscous oil is about 23%. The higher swelling factor for *n*-decane compared to the viscous oil is consistent with the expected higher CO2 solubility in the lighter oil.

The swelling factor for both oil types during CWI can also be estimated by measuring the size of an oil ganglion within the micromodel during CWI. Figure 13 shows a magnified image of an isolated trapped oil in a part of the micromodel before (A) and at the end of CWI (B) in the light oil experiment. Comparison of these two images demonstrate a considerable swelling of the oil and displacement of the water phase by both co-current and counter current flow mechanisms. The amount of oil swelling for *n*-decane based on these two pictures is estimated to be around 105% at the conditions of the experiments (2000 psia and 38 °C). Despite a small difference, this value is consistent with the 94% swelling factor obtained from the average oil saturation in the

porous medium. Figure 14 shows two snapshots of an oil ganglion during the heavy oil CWI test. The swelling factor from these images for the viscous oil estimated to be about 23%, which is exactly the same as the value obtained through average oil saturation in the micromodel.

## CONCLUSIONS

The following conclusions can be drawn based on the results of the experiments discussed in this paper:

- CWI as tertiary recovery method (post waterflood) increased oil recovery both for light and the viscous oil. However this increase was higher for the light oil (32.7%) than the viscous oil (11.82%). This was mainly due to a higher swelling factor in the light oil.
- Two main observed mechanisms of oil recovery during carbonated water injection were; the swelling and subsequent coalescence of trapped oil ganglia, local flow diversion and reduction of the oil viscosity.
- Significant oil swelling was observed. The swelling of the viscous oil and *n*-decane as a result of partitioning of CO2 from carbonated water and its dissolution in the oil, were estimated to be 23% and 105%, respectively.

## ACKNOWLEDGEMENTS

The Carbonated Water Injection (CWI) project at Heriot-Watt University is supported equally by: Total Exploration and Production UK, StatoilHydro, Dong Energy and Petrobras and the UK DECC (former DTI), which is gratefully acknowledged.

## REFERENCES

Bijeljic B. R., Muggeridge A. H., Blunt M. J: “Effect of Composition on Waterblocking for Multicomponent Gas floods’’ SPE 77697, SPE annual Technical Conference and Exhibition held in San Antonio, Texas, 29 Sep-2Oct 2002.

Campbell B. T., Orr, Jr F. M.: “Flow Visualization for CO2/Crude-Oil Displacements’’ SPE 11958, Oct 1985.

Chiquet, P. and Broseta, D.: ’’Capillary Alteration of Shaly Caprocks by Carbon Dioxide’’, SPE 94183, 2005.

Daoyong Y., Paitoon T., and Yongan G.: “Interfacial Tensions of the Crude Oil + Reservoir Brine + CO2Systems at Pressures up to 31 MPa and Temperatures of 27 °C and 58 °C’’, Journal of Chemical and Engineering Data, Vol. 50, No. 4, 2005.

Do H.D., Pinczewski W.V.: “Diffusion controlled swelling of reservoir oil by indirect contact with injection gas’’, Chemical Engineering Science, Vol.48, No18, PP. 3243-3252, 1993.

Grogan A.T., Pinczewski W.V.: “The Role of Molecular Diffusion Processes in Tertiary C02 Flooding’’, SPE 12706, May 1987.

Grogan A.T., Pinczewski W.V., Ruskauff G. J., Orr Jr F.M.: "Diffusion of CO2 at Reservoir Conditions: Models and Measurements'', SPE 14897, Feb 1988.

National Institute of Standard and Technology Website. "**http://www.nist.gov/srd/**''

Patel, P.D., Christman, R.G., and Gardner, J. W.: "An Investigation of Unexpectedly Low Field-Observed Fluid Mobilities during Some CO2 Tertiary Floods'', SPERE, Vol. 507, Nov 1987.

Philip Wylie and Kishore K. Mohanaty: "Effect of Water Saturation on Oil Recovery by Near-Miscible Gas Injection'', SPE paper 36718, Nov 1997.

Solomon, S.: "The Bellona Foundation- Fact sheet: CO2 Storage'' Bellona Report may 2007. **http://www.bellona.org/factsheets/1191921304.33**.

Sohrabi, M., Henderson, G.D., Tehrani, D.H. and Danesh, A.: "Visualisation of Oil Recovery by Water Alternating Gas (WAG) Injection Using High Pressure Micromodels - Water-Wet System'', SPE 63000, SPE Annual Technical Conference and Exhibition held in Dallas, Texas, 1–4 October 2000,.

Sohrabi, M, Tehrani, D H, Danesh, A. and Henderson, G.: "Visulisation of Oil Recovery by Water-Alternating-Gas Injection Using High-Pressure Micromodels'', SPEJ, 9, 290-301, 2004.

Sohrabi, M, Danesh, A., Tehrani, D. H and Jamiolahmady, M.: "Microscopic Mechanisms of Oil Recovery By Near-Miscible Gas Injection'' Transport in Porous Media, 72, 351-367, 2007.

Sohrabi M., Danesh A., and Jamiolahmady M.: "Visualisation of Residual Oil Recovery by Near-Miscible Gas and SWAG Injection Using High-Pressure Micromodels'', Transport in Porous Media, 74, 239-257, 2008a.

Sohrabi M., Riazi M., Jamiolahmady M., Ireland S. and Brown C.: "Carbonated Water Injection for Oil Recovery and CO2 Storage'', Sustainable Energy UK: Meeting the Science and Engineering Challenge Conference, Oxford University, 13-14 May 2008b.

Tumasyan, A. B., Panteleev, V. G. & Meinster, G. P.: "Influence de l'anhydride carbonique sur les proprieties physiques du petrole et de l'eau'', Nefteprom. dela, 2 (1969) 20-3).

Table 1: Dimensional Characteristic of the Micromodel.

| Length cm | Width cm | MM PV $cm^3$ | Ave. Pore depth $\mu m$ | Pore Dia. Range $\mu m$ |
|---|---|---|---|---|
| 3.8 | 0.7 | 0.01 | 50 | 30-500 |

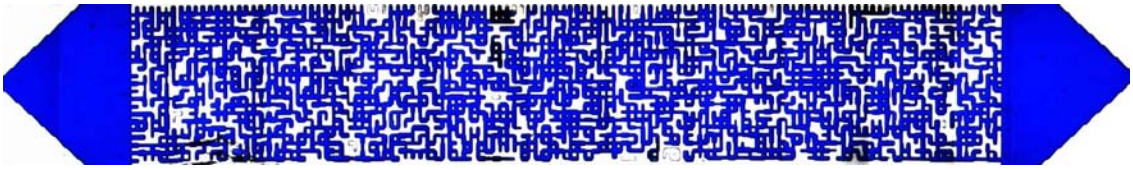

Figure 1: Image of the micromodel when fully saturated with blue-dyed water.

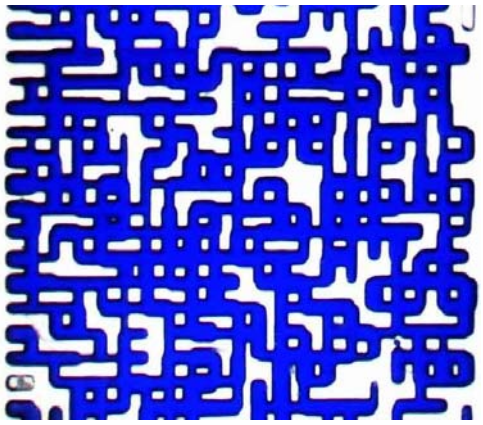

Figure 2: Pore pattern of the micromodel.

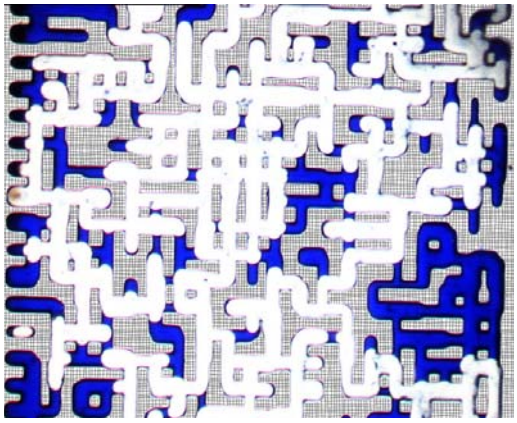

Figure 3: Initial oil saturation, light oil.

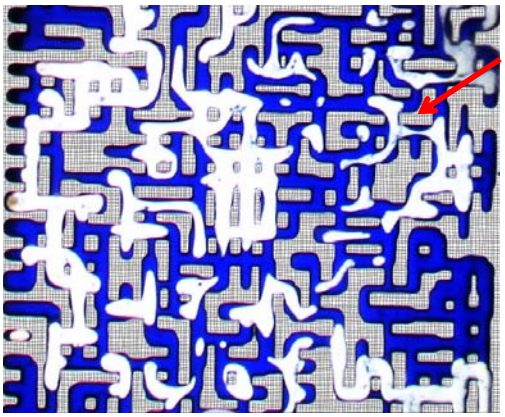

Figure 4: End of water injection, light oil.

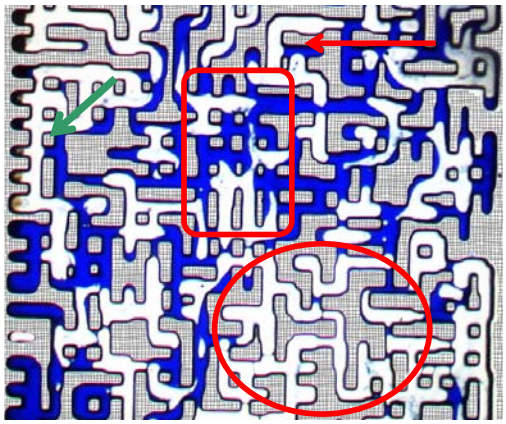

Figure 5: End of CWI stage, light oil.

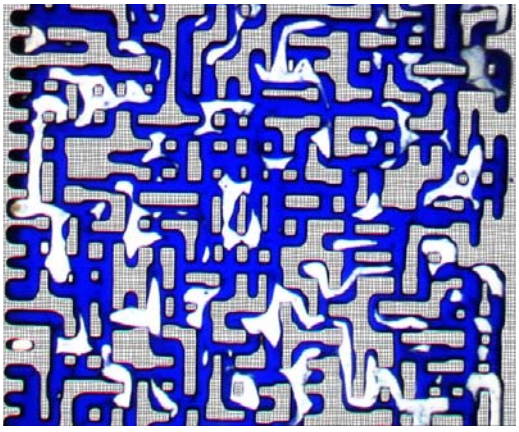

Figure 6: End of second WI period.

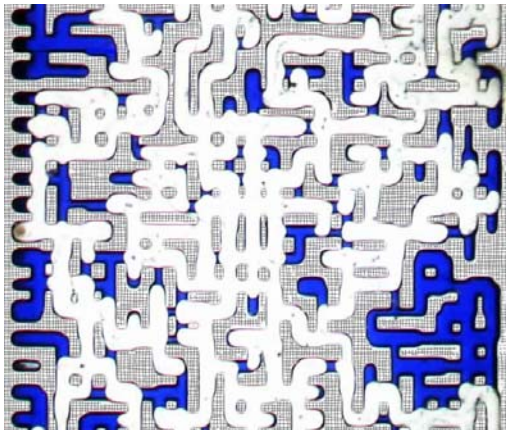

Figure 7: Initial oil saturation, viscous oil.

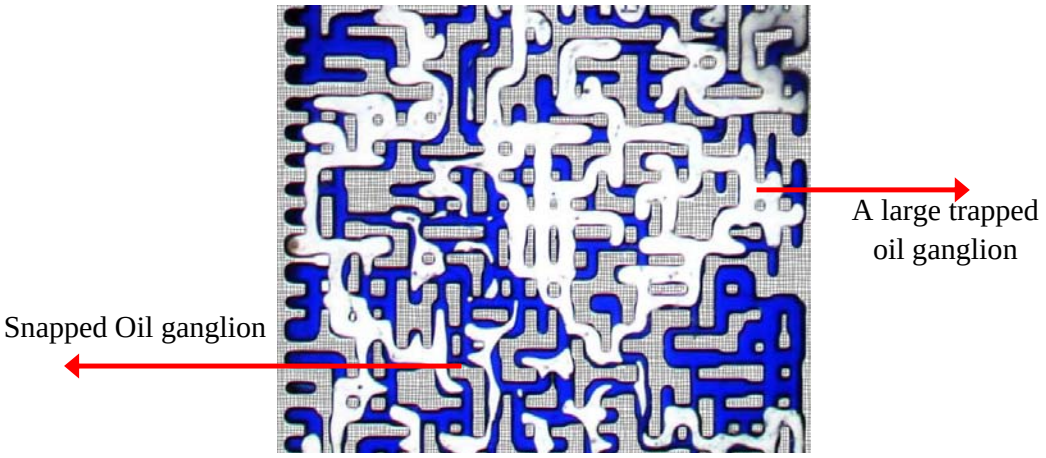


Figure 8: Fluid distribution after the first WI, viscous oil.

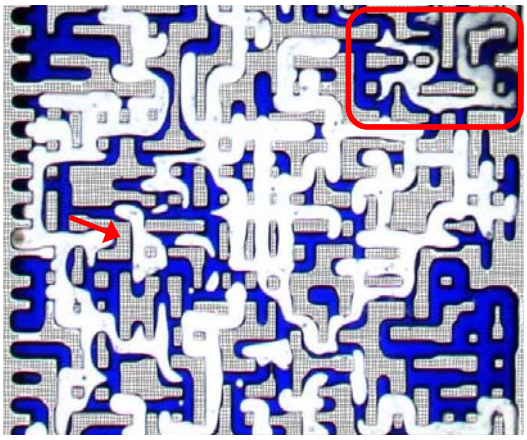

Figure 9: End of CWI stage, viscous oil.

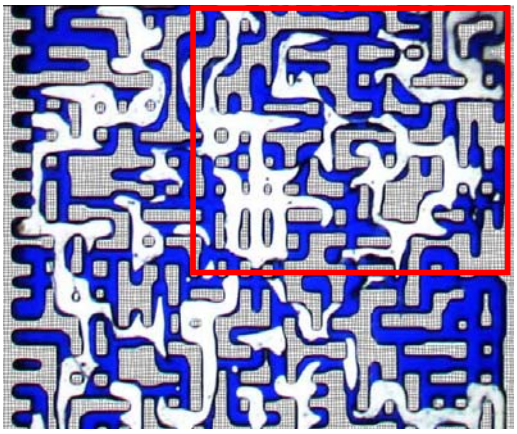

Figure 10: Second WI, viscous oil.

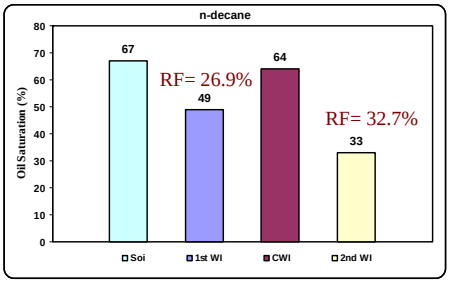


Figure 11: Oil saturation in the first test.

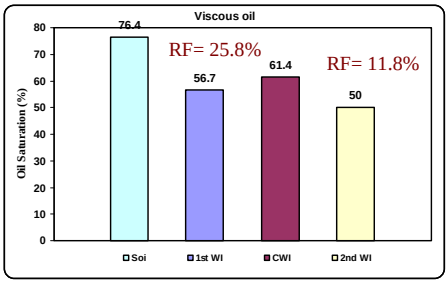


Figure 12: Oil saturation in the second test.

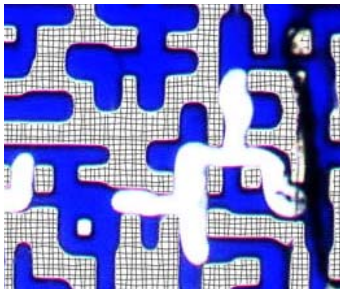
**A**

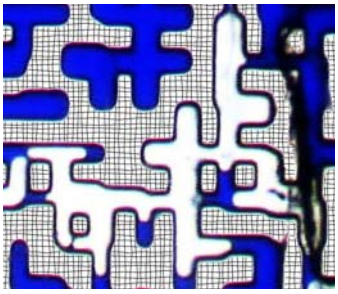
**B**

Figure 13: Swelling of an oil (n-Decane). **A)** End of the 1st WI **B)** end of CWI.

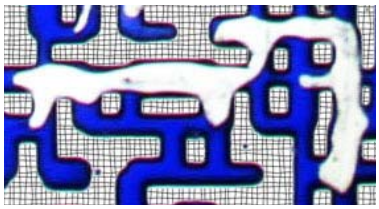
A

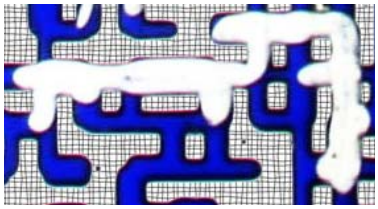
B

Figure 14: Swelling of an oil ganglion (viscous oil). **A)** End of the 1st WI **B)** end of CWI.